scientific reports

Check for updates

OPEN

Effect of synthesis conditions on the porous texture of activated carbons obtained from Tara Rubber by $FeCl_3$ activation

Mirosław Kwiatkowski[1]✉, Carolina Belver[2] & Jorge Bedia[2]

This paper presents the results of an unique analysis of the influence of the mass ratio of activator $FeCl_3$ to precursor and the temperature of the activation process on the formation of the porous structure of activated carbons obtained from Tara Rubber by $FeCl_3$ activation. The study used the new numerical clustering based adsorption analysis method and the quenched solid density functional theory, taking into account, among other things, the heterogeneity of the analysed surface which is a new approach rarely used in the analysis of the porous structure of adsorbents. On the basis of the calculation results, it was concluded that the activated carbon with the most developed porous texture was obtained at a mass ratio ($FeCl_3$:Tara Rubber) of 2, at an activation process temperature of 800 °C. This activated carbon is also characterised by the lowest degree of surface heterogeneity and at the same time, however, the widest range of micropores compared to activated carbons obtained at other mass ratios. The analyses carried out further demonstrated the valuable and complementary information obtained from the structure analysis methods and their high utility in practical applications, especially in the development of new industrial technologies for the production of adsorbents and the selection of optimal conditions for their production.

Owing to their unique properties, such as high specific surface area and pore volume, as well as the substantial advantage of controlling their porous structure through the selection of suitable raw materials and production technologies, microporous carbonaceous adsorbents are in common use in industrial processes and everyday life. Activated carbons are used mainly for adsorption processes[1–5], although they are also widely used in catalysis, both as mass catalysts[6–9] or as catalysts supports[10–13] or in energy applications[14,15]. They are usually obtained by physical activation preceded by carbonisation, or by chemical activation[16].

Carbonisation is performed by heat treatment at high temperature in an inert atmosphere. During this process, volatiles are removed and char is consequently enriched in elemental carbon[17,18]. The efficiency of the carbonisation process is influenced by the final process temperature, the rate of temperature rise, the inert gas flow rate and the duration of the process[19,20]. The highest mass yield of the carbonisation process is achieved at relatively low temperatures and low heating rates. The char, product of the carbonisation process, has a poorly developed porous structure and a low specific surface area, as the pores are blocked by tarry substances and must therefore undergo an additional physical or chemical activation process[21]. During the above-mentioned processes, the pore-blocking tarry substances are removed and new pores are formed, and consequently, the porous structure, especially the micropores, develops further[22].

Physical activation can be a one-step process or, more often, a two-step process, i.e. preceded by carbonisation of the raw material, and involves activation of the raw material or char with an oxidising gas at a high temperature, i.e. around 800–1100 °C[23,24]. Carbon dioxide and steam, possibly air (in this case a lower activation temperature is used), are predominantly used as an oxidising gas[23–25]. The extent to which a porous structure develops during physical activation depends mainly on the temperature and duration of the process as well as the reactivity of the gasification agent[26]. The use of carbon dioxide as an activator leads to the formation of predominantly micro- and ultra-microporous structures, while steam activation leads to the development of a wider pore distribution and a higher proportion of mesopores. The main advantages of physical activation include the low cost of producing activated carbons and the ability to retain the shape and texture of the precursor. Physical

[1]Department of Fuel Technology, Faculty of Energy and Fuels, AGH University of Krakow, al. Adama Mickiewicza, 30, 30-059 Krakow, Poland. [2]Departamento de Ingeniería Química, Facultad de Ciencias, Universidad Autónoma de Madrid, Campus Cantoblanco, 28049 Madrid, Spain. ✉email: kwiatkow@agh.edu.pl

activation therefore makes it possible to produce low-abrasion activated carbons from hard raw materials such as nut shells and fruit stones, as well as to produce activated nonwovens and fabrics and carbon mats from fibrous precursors[26].

Chemical activation can, by analogy with physical activation, be a one-step process or a two-step process preceded by carbonisation in the case of obtaining activated carbons from biomass by chemical activation using NaOH or KOH as activator[27–37], as otherwise these strong bases may dissolve the organic matter of the precursor, making subsequent activation impossible. Compared to physical activation, chemical activation allows better development of surfaces and microporous structures and is less energy-intensive due to the lower process temperature and its shorter time[38,39]. Chemical activation, however, requires an additional washing process of the final product to remove residues of the activator used. Furthermore, from an environmental point of view, hydroxides and alkali metal acids are less favourable as activators because they are highly corrosive and toxic. As a result, other safer activators such as sodium amide $NaNH_2$[40] are increasingly being used alternatively and new methods of producing activated carbons as well as new activators are also being sought and the use of ferric chloride $FeCl_3$ as an activator is of particular interest[41]. The use of $FeCl_3$ as an activator has a number of advantages over other commonly used activators used in the production of activated carbons, among which are the lower environmental impact as well as the lower cost[41]. This is due to the fact that the use of $FeCl_3$ as an activator does not require stringent safety measures and suitable materials for corrosion-resistant plant construction. In addition, a unique feature of activation with $FeCl_3$ is the possibility of obtaining activated carbons with very well-developed porosity and a relatively large surface area that are also characterised by magnetic properties[41,42]. In this sense, this study analyses the influence of the mass ratio of activator $FeCl_3$ to precursor and the temperature of the activation on the formation of the porous structure of activated carbons obtained from Tara Rubber by $FeCl_3$ chemical activation. The precise knowledge of the porosity of activated carbons will help to the improvement of current applications and even to the development of new ones in which a tailored porosity would be needed. In this sense, this research could help to the detailed description of the porosity of activated carbons, providing complementary information about the porosity of these materials.

Materials and methods

The work of Bedia, and co-workers[42] presents the unique results of analyses of activated carbons obtained from Tara gum by chemical activation using $FeCl_3$ as activator. These activated carbons were obtained at different activation temperatures (400–1000 °C) and at different mass ratios of activator to precursor ($FeCl_3$:Tara gum, $r = 0.5$, 1, 2 and 3) obtained by physical mixing. Briefly, initially Tara gum and iron chloride were physically mixed. The mixture was maintained overnight in an oven at 60 °C and then pyrolyzed in a horizontal tube furnace for two hours under continuous N_2 flow of 150 cm^3 min^{-1} (n.c.). that was maintained until the furnace was cooled down. It was then washed, firstly with aqueous HCl (0.1 N) at 70 °C during and then with distilled water at room temperature up to neutral pH. The final samples were dried overnight in an oven at 60 °C. The activated carbons were denoted by the letters "GT", followed by the impregnation ratio and the activation temperature in degrees Celsius (i.e. GT2-800 is the activated carbon prepared with an impregnation ratio of 2 and at an activation temperature of 800 °C). The resulting activated carbons showed a well-developed porous texture, mainly in terms of micropores size, and a superparamagnetic character due to the presence of iron forms in their structure[42]. However, the Brunauer–Emmett–Teller (BET)[43] and t-plot methods[44] as well as the Barrett-Joyner-Halenda (BJH) method[45] for the determination of pore size distributions used in the analysis of porous structure, are criticised for over-simplifying assumptions that deviate significantly from reality without taking into account surface heterogeneities. With the development of the science of physicochemical processes on the surface of solids, significant progress has been made in understanding the mechanisms of adsorption and consequently, a solid theoretical basis for characterising the adsorption process has been developed. This progress is largely related to the application of methods such as Density Functional Theory (DFT), which allows the adsorption and phase behaviour of pore fluids to be described at the molecular level[46].

The Non Localized Density Functional Theory (NLDFT) method, based on a model of independent gap-shaped pores with ideal graphite walls, has become particularly popular. However, such a model has a significant drawback; starting from a pore width greater than a few molecular diameters, the theoretical adsorption isotherms show many steps associated with layer transitions related to the formation of a monolayer, a second adsorbed layer and so on[47]. Experimentally, however, stepped adsorption isotherms are only obtained at low temperatures for fluids adsorbed on molecularly smooth surfaces. In activated carbons, transitions between layers are hampered by the inherent energetic and geometric heterogeneities of their actual surfaces. The layering steps on the theoretical isotherms cause artificial gaps in the calculated Pore Size Distributions (PSD). Such a discrepancy between the theoretical assumption of a smooth and homogeneous surface and the experimental situation is particularly significant for microporous carbon adsorbents with wide PSDs. The aforementioned problems were solved by the development of a Quenched Solid Density Functional Theory (QSDFT) model that quantifies the geometric heterogeneity of a surface through the roughness parameter[48]. This parameter represents half the width of the range of undulations at the molecular level of the pore wall surface. The aforementioned roughness parameter can be determined by comparing theoretical and experimental adsorption isotherms on the reference surface. The QSDFT method provides a significant improvement over traditional DFT methods as well as the NLDFT method, which assume pore walls as homogeneous graphite-like flat surfaces.

A next novel approach for the analysis of the surface properties of materials is the numerical clustering-based adsorption analysis (LBET) method[49,50]. Compared to the conventional methods, the LBET method considers the heterogeneity of the surface and allows the determination of the size and shape of the adsorbate molecule clusters formed, the adsorption energy distributions (AEDs), and the reliability and credibility of the obtained results[49,50].

The LBET and QSDFT methods not only provide much more reliable results, but also much more information about the analysed structure. Consequently, the concept of carrying out a new extended cycle of analysis using LBET and QSDFT methods, taking into account, among other things, the heterogeneity of the surface, was developed. The analyses carried out comprehensively considered the effects of activation process temperature and activator/precursor mass ratio (i.e. $FeCl_3$:Tara Rubber), on the formation of the porous structure of the resulting activated carbons.

Discussion of the obtained results

The results of the analyses carried out using the LBET and QSDFT methods are summarised in Tables 1, 2 and shown in Figs. 1, 2. The results of calculations for activated carbon GT2-400, i.e. obtained by chemical activation using $FeCl_3$ as activator at a mass ratio of activator to precursor ($FeCl_3$:Tara Rubber) equal to 2 and at 400 °C, allow us to conclude that in the micropores of the material studied there are limitations to the growth of nitrogen molecule clusters associated with the competitive expansion of neighbouring clusters, as indicated by the number of the best-fit mathematical model of the adsorption process. The surface of GT2-400 activated carbon is moderately heterogeneous, as indicated by the value of the surface heterogeneity parameter h ($h = 3$).

GT2-400 activated carbon has a poorly developed porous structure, as indicated by the value of the volume parameter of the first adsorbed layer V_{hA} ($V_{hA} = 0.157$ cm^3/g) and the values of the S_{QSDFT}, V_{QSDFT} parameters, *i.e.* specific surface area and pore volume, respectively, determined using the QSDFT method ($S_{QSDFT} = 362$ m^2/g, $V_{QSDFT} = 0.213$ cm^3/g). In the pores of this material, low and significantly branching clusters of nitrogen molecules form, as indicated by the values of the geometrical parameters of the LBET model, i.e. the heights of the adsorbate clusters α and their width β ($\alpha = 0.34$, and $\beta = 3.10$). In turn, the values of the energy parameters Q_A/RT and B_C indicate preferential conditions for the multilayer adsorption process ($Q_A/RT = -7.68$ and $B_C = 6.83$).

It is noteworthy that, despite a very good fit of the theoretical isotherm to the empirical isotherm, as indicated by the dispersion value of the fit error $\sigma_e = 0.23$, the value of the traceability parameter w_{id} ($w_{id} = 0.29$), may indicate the presence of some deviations of the actual structure from the assumptions made in the structure model implemented in the LBET method. Another material analysed was the GT2-600 activated carbon sample obtained at a mass ratio of $r = 2$, at an activation temperature of 600 °C in contrast to the previously analysed GT2-400 activated carbon, this material shows geometric limitations to the growth of clusters of adsorbate molecules as indicated by the number on a better-fitting cluster mathematical model of the adsorption process.

Activated carbon GT2-600 is characterised by moderate surface heterogeneity, similar to activated carbon GT2-400. However, the higher value of the V_{ha} parameter, i.e. the volume of the first adsorbed layer ($V_{ha} = 0.428$ cm^3/g), as well as the S_{QSDFT} and V_{QSDFT} parameters ($S_{QSDFT} = 879$ m^2/g and $V_{QSDFT} = 0.517$ cm^3/g), indicates a greater development of the microporous structure. The value of the geometrical parameter for the height of clusters of adsorbate molecules α is, however, lower ($\alpha = 0.26$) compared to the previously analysed material, indicating the formation of lower clusters of nitrogen molecules in the micropores of activated carbon GT2-600 compared to activated carbon obtained at a lower temperature, and thus the greater presence of small

Material	*Model No*	h	V_{hA} [cm^3/g]	α	β	Q_A/RT	B_C	σ_e	w_{id}	S_{QSDFT} [m^2/g]	V_{QSDFT} [cm^3/g]	S_{BET} [m^2/g]	V_p [cm^3/g]
GT2-400	5	3	0.157	0.3	3.1	−7.68	6.8	0.2	0.2	362	0.213	379	0.245
GT2-600	21	3	0.428	0.2	3.1	−6.54	5.6	0.1	0.5	879	0.517	996	0.582
GT2-800	3	2	1.018	0.7	1.0	−8.67	6.5	0.8	0.2	1439	0.879	1680	0.990
GT2-1000	19	3	0.601	0.6	1.8	−8.26	7.7	0.5	0.3	1113	0.702	1298	0.810

Table 1. The results of the analysis of a porous structure of activated carbons prepared via chemical activation using $FeCl_3$ as activator at different temperatures of the activation process, i.e. 400, 600, 800 and 1000 °C, based on nitrogen adsorption isotherms, using the LBET and QSDFT methods. V_{hA} is the volume of the first adsorbed layer, Q_A/RT is the dimensionless energy parameter for the first adsorbed layer; B_C is the energy parameter for the higher adsorbed layers; α is the geometrical parameter of the porous structure determining the height of the adsorbate molecule clusters; β is the geometrical parameter of the porous structure determining the width of the adsorbate molecule clusters; h is the surface heterogeneity parameter; S_{QSDFT} is the micropores specific surface area; V_{QSDFT} is the volume of micropores; S_{BET} is the BET surface area and V_p is the total pore volume, both obtained for the experimental N_2 adsorption–desorption isotherms.

Material	*Model No*	h	V_{hA} [cm^3/g]	α	β	Q_A/RT	B_C	σ_e	w_{id}	S_{QSDFT} [m^2/g]	V_{QSDFT} [cm^3/g]
GT05-800	4	3	0.463	0.42	3.19	−7.68	7.40	0.42	0.26	940	0.634
GT1-800	3	2	0.781	0.70	1.00	−7.93	7.73	0.61	0.13	1075	0.657
GT2-800	3	2	1.018	0.74	1.00	−8.67	6.55	0.87	0.28	1439	0.879
GT3-800	6	3	0.534	0.26	2.75	−7.15	7.73	0.58	0.04	1074	0.623

Table 2. The results of the analysis of a porous structure of activated carbons prepared via chemical activation using $FeCl_3$ as activator at different mass ratios of activator to precursor ($FeCl_3$:Tara gum, $r = 0.5$, 1, 2 and 3), based on nitrogen adsorption isotherms, using the LBET and QSDFT methods.

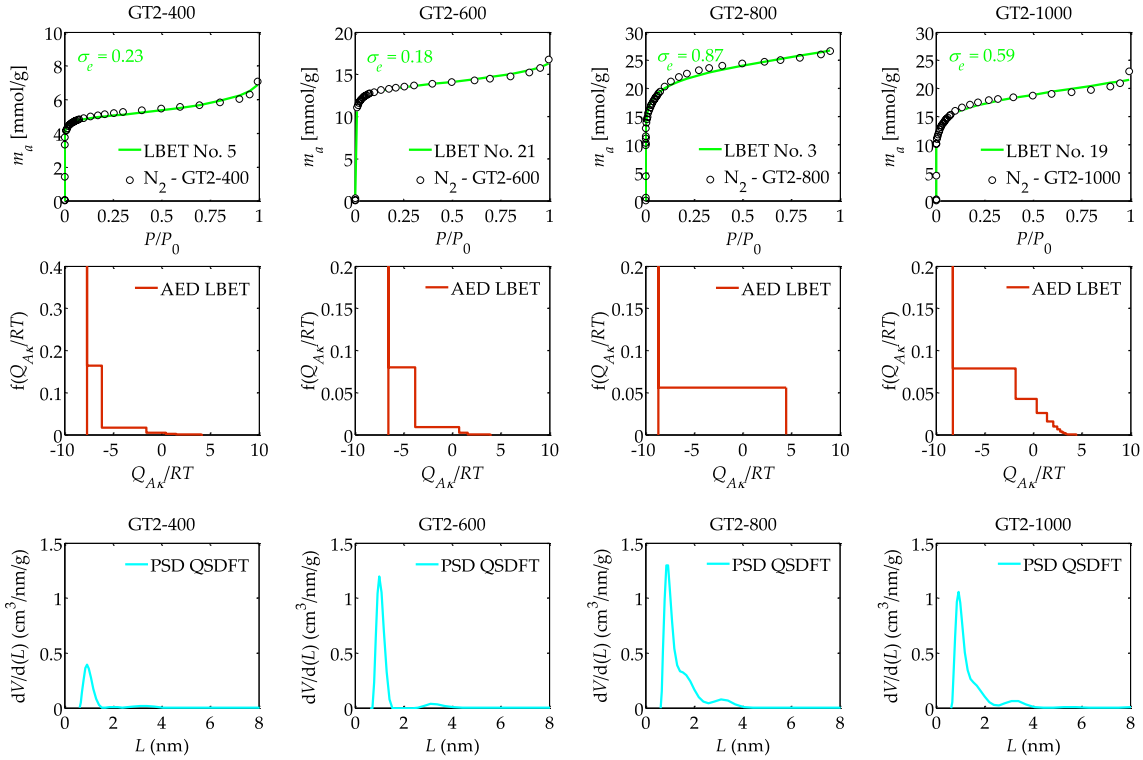

Figure 1. The nitrogen adsorption isotherms and the results of the identification of the adsorption systems via the LBET and QSDFT methods: where AED is the adsorption energy distributions, and PSD is the pore size distributions obtained for the activated carbons prepared via chemical activation using $FeCl_3$ as activator at different temperatures of the activation process, i.e. 400, 600, 800 and 1000 °C.

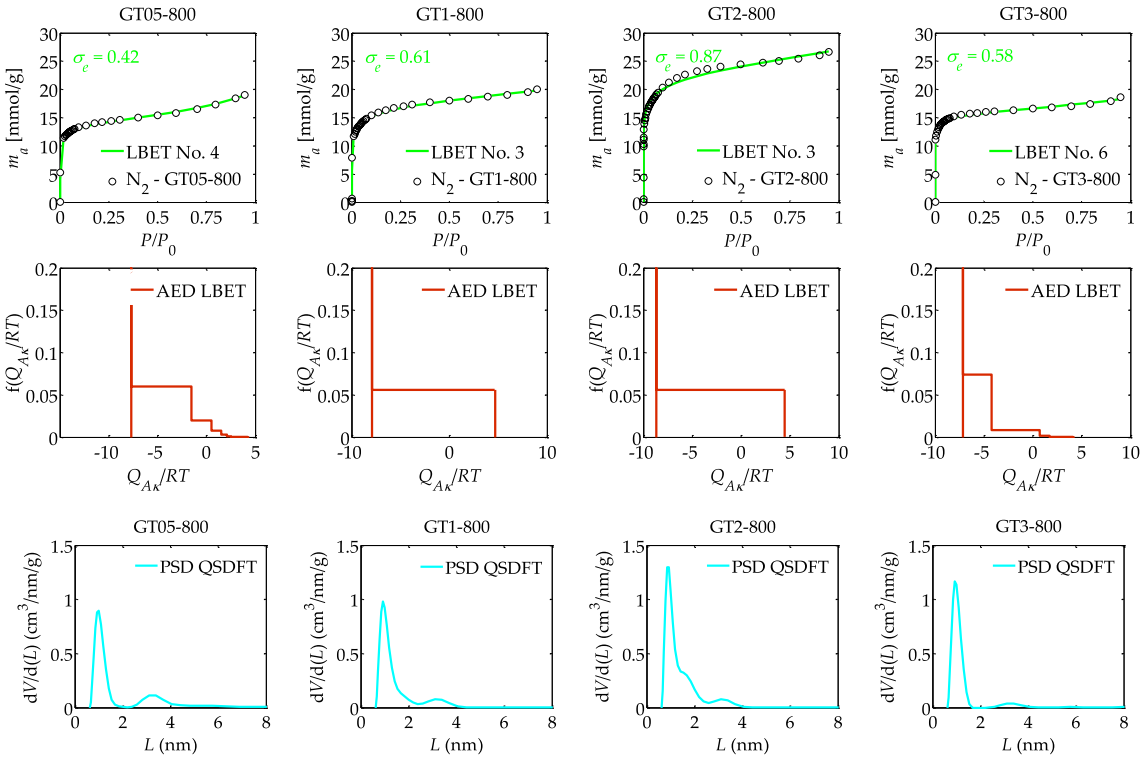

Figure 2. The nitrogen adsorption isotherms and the results of the identification of the adsorption systems via the LBET and QSDFT methods: where AED is the adsorption energy distributions, and PSD is the pore size distributions obtained for the activated carbons prepared via chemical activation using $FeCl_3$ as activator at different mass ratios of activator to precursor ($FeCl_3$:Tara gum, r = 0.5, 1, 2 and 3).

micropores in the pore structure of this material. In the case of sample GT2-600, the very good identifiability of the adsorption system, and thus the high reliability of the determined porous structure parameters, is noteworthy.

The next activated carbon sample analysed, designated GT2-800 and therefore obtained at a mass ratio of $r = 2$ and at an activation temperature of 800 °C, is characterised by limitations on the expansion of nitrogen molecule clusters due to the competitive expansion of neighbouring clusters. The sample is also characterised by the lowest degree of surface heterogeneity among the analysed activated carbons obtained at an impregnation mass ratio of 2. Activated carbon GT2-800 also had the most developed porous structure, as indicated by the very high value of the volume of the first adsorbed layer V_{hA} ($V_{hA} = 1.018$ cm^3/g), the very high value of the S_{QSDFT} and V_{QSDFT} parameters ($S_{QSDFT} = 1439$ m^2/g, and $V_{QSDFT} = 0.879$ cm^3/g) and the high height of the clusters of adsorbate molecules, as indicated by the value of the geometrical parameter α ($\alpha = 0.74$). In turn, the value of the geometrical parameter β indicates that non-branching clusters of adsorbate molecules are formed in the pores of the analysed sample. Of note is the average identifiability of the N_2—GT2-800 adsorption system, indicating the presence of some deviations from the theoretical model of the porous structure from the actual pore structure of the analysed material.

Analysis of a further sample of GT2-1000 activated carbon obtained at an activator/precursor mass ratio of 2 and an activation temperature of 1000 °C, showed limitations in the growth of clusters of adsorbate molecules associated with geometrical pore limitations and destruction of the porous structure associated with a too high activation temperature, as indicated by significantly lower values of the V_{hA} parameters, S_{QSDFT} and V_{QSDFT} parameters and α in comparison with the values of these porous structure parameters determined for GT2-800 activated carbon obtained at a lower temperature, i.e. 800 °C. The increase of the activation temperature from 800 to 1000 °C produces a significantly deeper devolatilization of the organic precursor. This results in an increase of the ash content of the sample[42] and consequently to a decrease in the porosity of the sample, since ashes are essentially non-porous.

The shapes of the graphs of AED adsorption energy distributions on the surface of the analysed activated carbons determined by the LBET method, shown in Fig. 1, indicate the occurrence in the analysed samples of a significant proportion of sites with equal energy, i.e. micropores in which single nitrogen molecules adsorb, and the occurrence of a significant proportion of sites with a wide range of adsorption energies.

It is also noteworthy that activated carbon GT2-800, in contrast to the other analysed samples obtained at a mass ratio of $r = 2$, is characterized by a uniform distribution of sites with a wider energy range and thus the lowest surface energy heterogeneities. Pore size distributions were also determined for the carbons analysed using the QSDFT method, the shape of which indicates the predominant share of micropores in the total porosity of the activated carbons analysed, and some small share of small mesopores. It is noteworthy the smallest volume of micropores obtained for sample GT2-400 (see Fig. 1).

The study also analysed the effect of the mass ratio of activator to precursor on the formation of the porous structure of activated carbons obtained from Tara Rubber using $FeCl_3$ as activator at mass ratios from $r = 0.5$–3. The results of the analyses using the LBET and QSDFT methods are shown in Table 2 and Fig. 2.

Analysis of the results obtained for GT05-800 activated carbon showed that the limitations of nitrogen molecule cluster expansion are due to the competitive expansion of neighbouring clusters. The surface area of GT05-800 activated carbon is moderately heterogeneous, as indicated by the value of the parameter $h = 3$, and the values of the parameters V_{hA}, α, S_{QSDFT}, V_{QSDFT} ($V_{hA} = 0.463$ cm^3/g, $\alpha = 0.42$, $S_{QSDFT} = 940$ m^2/g, $V_{QSDFT} = 0.634$ cm^3/g) indicate good development of the porous structure.

The value of the geometrical parameter of the cluster width β, indicates the presence of significantly branched clusters of nitrogen molecules ($\beta = 3.19$) in the pores of the analysed material. The values of the energy parameters Q_A/RT and B_C ($Q_A/RT = -7.68$ and $B_C = 7.40$) indicate preferential conditions for the multilayer adsorption process to take place. Only the average fit of the theoretical isotherm to the empirical data is noteworthy, and thus also the average traceability of the absorption system indicating the occurrence of some deviations of the porous structure from the assumed model pore structure in the LBET method.

The next sample analysed was an activated carbon sample designated GT1-800, i.e. a material obtained at an activator/precursor ($FeCl_3$:Tara Rubber) mass ratio of 2, at an activation temperature of 800 °C. This sample is characterised by a lower degree of surface heterogeneity as indicated by the value of the surface heterogeneity parameter h ($h = 2$) as well as a more developed porous structure as indicated by the values of the parameters V_{hA}, α, S_{QSDFT} and V_{QSDFT}. High non-branching clusters of adsorbate molecules form in the pores of the activated carbon, as indicated by the values of the geometric parameters α and β ($\alpha = 0.70$, and $\beta = 1.00$).

The results of the analysis of a further GT2-800 activated carbon sample obtained at a mass ratio of 2, at an activation temperature of 800 °C, which has already been described in detail above. In summary, this sample shows the most developed microporous structure, as indicated by the highest values of the V_{hA}, α, S_{QSDFT} and V_{QSDFT} parameters, of all the activated carbons analysed throughout the study cycle. Further increasing the mass ratio of activator to precursor, i.e. to $r = 3$ in the case of activated carbon GT3-800 resulted in the destruction of the porous structure, as indicated by significantly lower values of the V_{hA} parameters, α, S_{QSDFT} and V_{QSDFT}.

The shapes of the energy distribution diagrams of AED adsorption on the surface of the analysed activated carbons determined by the LBET method, shown in Fig. 2, indicate the predominance of sites with equal energy in all activated carbon samples, which allows the presence of micropores in which single nitrogen molecules adsorb to be inferred. Activated carbon GT3-800 has, as can be seen, the narrowest adsorption energy distribution on the surface. On the other hand, the analysis of the pore size distributions determined for the activated carbons analysed and presented in Fig. 2, indicate that the average size of the micropores contributed to the total porosity of the activated carbons analysed.

Conclusions

The analytical results presented here are a significant and unique extension of previous studies and have provided a lot of new reliable information on activated carbons obtained at different activation temperatures and at equal mass ratios, thus providing the opportunity to determine the optimum process conditions for producing an activated carbon dedicated to a specific adsorption process. On the basis of the study, it was shown that, among the various synthesis conditions, the activation temperature and, to a lesser extent, the mass ratio of activator to precursor are the most significant parameters affecting the final properties of the activated carbons obtained. On the basis of the calculation and analysis results obtained, it was shown that activated carbon with the highest porous structure development was obtained at a mass ratio ($FeCl_3$:Tara Rubber) of 2, at an activation process temperature of 800 °C. This activated carbon is also characterised by the lowest degree of surface heterogeneity and at the same time, however, the widest range of micropores compared to activated carbons obtained at other activator/precursor mass ratios. The analysis also demonstrated the mutual complementarity of the LBET and QSDFT methods, which, through their simultaneous application, enable a comprehensive and reliable analysis of the porous structure taking into account, among other things, surface heterogeneities. This method, together with appropriate economic analysis, helps the precise selection of the method and conditions of the process of obtaining activated carbons at specific costs of the manufacturing process, and thus makes it possible to obtain materials that can successfully compete with other technologies used in industrial practice and everyday life.

Data availability

All data generated or analysed during this study are included in this published article.

Received: 6 November 2023; Accepted: 14 January 2024
Published online: 27 January 2024

References

1. El-Bery, H. M., Saleh, M., El-Gendy, R. A., Saleh, M. R. & Thabet, S. M. High adsorption capacity of phenol and methylene blue using activated carbon derived from lignocellulosic agriculture wastes. *Sci. Rep.* **12**, 5499. https://doi.org/10.1038/s41598-022-09475-4 (2022).
2. Chimanlal, I., Lesaoana, M. & Richards, H. Chemical modification of Macadamia-derived activated carbon for remediation of selected heavy metals from wastewater. *Miner. Eng.* **184**, 107663. https://doi.org/10.1016/j.mineng.2022.107663 (2022).
3. Fito, J. *et al.* Adsorption of methylene blue from textile industrial wastewater using activated carbon developed from Rumex abyssinicus plant. *Sci. Rep.* **13**, 5427. https://doi.org/10.1038/s41598-023-32341-w (2023).
4. Wang, S. *et al.* Hydrothermal pretreatment of KOH for the preparation of PAC and its adsorption on TC. *Materials* **16**, 4966. https://doi.org/10.3390/ma16144966 (2023).
5. Reaad, S., Moniem, R., Dadoosh, B. E., Jasim, A. N. A. A. & Hussain, A. S. Activated carbon nanoparticles as adsorbent to remove the cadmium ion from aqueous solution thermodynamic study. *Al-Mustansiriyah J. Sci.* **34**, 44–49. https://doi.org/10.23851/mjs.v34i2.1260 (2023).
6. Yang, J. *et al.* Recent developments in activated carbon catalysts based on pore size regulation in the application of catalytic ozonation. *Catalysts* **12**, 1085. https://doi.org/10.3390/catal12101085 (2022).
7. Chen, H.-Y. & Lo, I.-T. Theoretical and experimental adsorption of silica gel and activated carbon onto chlorinated organic compounds in water: a case study on the remediation assessment of a contaminated groundwater site. *Appl. Sci.* **12**, 11955. https://doi.org/10.3390/app122311955 (2022).
8. He, H. *et al.* Porous carbon nanofibers derived from silk fibroin through electrospinning as N-doped metal-free catalysts for hydrogen evolution reaction in acidic and alkaline solutions. *ACS Appl. Mater. Interfaces* **14**, 834–849. https://doi.org/10.1021/acsami.1c19334 (2022).
9. Mergbi, M. *et al.* Valorization of lignocellulosic biomass into sustainable materials for adsorption and photocatalytic applications in water and air remediation. *Environ. Sci. Pollut. Res.* **30**, 74544–74574. https://doi.org/10.1007/s11356-023-27484-2 (2023).
10. Karaoğlu, K., Özçifçi, Z., Çalıªkan, M., Baran, T. & Akçay, H. T. Catalytic activity of palladium doped activated carbon from waste coffee on some environmental pollutants. *Mater. Chem. Phys.* **282**, 125857. https://doi.org/10.1016/j.matchemphys.2022.125857 (2022).
11. Guillén, E. *et al.* Pd-activated carbon catalysts for hydrogenation and Suzuki reactions. *Appl. Catal. A General* **368**, 113–120. https://doi.org/10.1016/j.apcata.2009.08.016 (2009).
12. Martin-Martinez, M., Gómez-Sainero, L. M., Bedia, J., Arevalo-Bastante, A. & Rodriguez, J. J. Enhanced activity of carbon-supported Pd-Pt catalysts in the hydrodechlorination of dichloromethane. *Appl. Catal. B Environ.* **184**, 55–63. https://doi.org/10.1016/j.apcatb.2015.11.016 (2016).
13. Lemus, J. *et al.* Improved synthesis and hydrothermal stability of Pt/C catalysts based on size-controlled nanoparticles. *Catal. Sci. Technol.* **6**, 5196–5206. https://doi.org/10.1039/C6CY00403B (2016).
14. Choudhary, R., Pandey, O. P. & Brar, L. K. Influence of thermal treatment atmosphere on N-doped carbon spheres for wastewater treatment and supercapacitor applications. *Mater. Chem. Phys.* **284**, 126037. https://doi.org/10.1016/j.matchemphys.2022.126037 (2022).
15. Li, Zh. *et al.* Hydrothermal synthesis of 3D hierarchical ordered porous carbon from yam biowastes for enhanced supercapacitor performance. *Chem. Eng. Sci.* **252**, 117514. https://doi.org/10.1016/j.ces.2022.117514 (2022).
16. Wei, Q. *et al.* Preparation and electrochemical performance of orange peel based-activated carbons activated by different activators. *Colloids Surf. A Physicochem. Eng. Aspects* **574**, 221–227. https://doi.org/10.1016/j.colsurfa.2019.04.065 (2019).
17. Mopoung, S. & Dejang, N. Activated carbon preparation from eucalyptus wood chips using continuous carbonization–steam activation process in a batch intermittent rotary kiln. *Sci. Rep.* **11**, 13948. https://doi.org/10.1038/s41598-021-93249-x (2021).
18. Goel, C., Mohan, S. & Dinesha, P. CO_2 capture by adsorption on biomass-derived activated char: A review. *Sci. Total Environ.* **798**, 149296. https://doi.org/10.1016/j.scitotenv.2021.149296 (2021).
19. Alfattani, R., Shah, M. A., Siddiqui, M. I. H., Ali, M. A. & Alnaser, I. A. Bio-char characterization produced from walnut shell biomass through slow pyrolysis: Sustainable for soil amendment and an alternate bio-fuel. *Energies* **15**, 1. https://doi.org/10.3390/en15010001 (2022).
20. Mokrzycki, J., Magdziarz, A. & Rutkowski, P. The influence of the Miscanthus giganteus pyrolysis temperature on the application of obtained biochars as solid biofuels and precursors of high surface area activated carbons. *Biomass Bioenergy* **164**, 106550. https://doi.org/10.1016/j.biombioe.2022.106550 (2022).
21. Trinh, T. K. *et al.* Carbonization and H_3PO_4 activation of fern *Dicranopteris linearis* and electrochemical properties for electric double layer capacitor electrode. *Sci. Rep.* **10**, 19974. https://doi.org/10.1038/s41598-020-77099-7 (2020).

22. Panwar, N. L. & Pawar, A. Influence of activation conditions on the physicochemical properties of activated biochar: a review. *Biomass Conv. Bioref.* **12**, 925–947. https://doi.org/10.1007/s13399-020-00870-3 (2022).
23. De Castro, P. M. *et al.* Preparation and characterization of steam and CO_2 activated carbon from Brazil nut shell. *Biosci. J.* **39**, 39054. https://doi.org/10.14393/BJ-v39n0a2023-64438 (2023).
24. Mai, N. T., Nguyen, M. N., Tsubota, T., Nguyen, P. L. T. & Nguyen, N. H. Evolution of physico-chemical properties of *Dicranopteris linearis*-derived activated carbon under various physical activation atmospheres. *Sci. Rep.* **11**, 14430. https://doi.org/10.1038/s41598-021-93934-x (2021).
25. Longo, L. *et al.* Waste biomasses as precursors of catalytic supports in benzaldehyde hydrogenation. *Catal. Today* **420**, 114038. https://doi.org/10.1016/j.cattod.2023.02.015 (2023).
26. Li, C. *et al.* Biomass-derived volatiles for activation of the biochar of same origin. *Fuel* **332**, 126034. https://doi.org/10.1016/j.fuel.2022.126034 (2023).
27. Sultan, H., Ahmed, N., Mubashir, M. & Danish, S. Chemical production of acidified activated carbon and its influences on soil fertility comparative to thermo-pyrolyzed biochar. *Sci. Rep.* **10**, 595. https://doi.org/10.1038/s41598-020-57535-4 (2020).
28. Kwiatkowski, M., Broniek, E., Fierro, V. & Celzard, A. An evaluation of the impact of the amount of potassium hydroxide on the porous structure development of activated carbons. *Materials* **14**, 2045. https://doi.org/10.3390/ma14082045 (2021).
29. Shao, J., Ma, C., Zhao, J., Wang, L. & Hu, X. Effective nitrogen and sulfur co-doped porous carbonaceous CO_2 adsorbents derived from amino acid. *Colloids Surf. A Physicochem. Eng. Aspects* **632**, 127750. https://doi.org/10.1016/j.colsurfa.2021.127750 (2022).
30. Li, S. *et al.* Investigation on pore structure regulation of activated carbon derived from sargassum and its application in supercapacitor. *Sci. Rep.* **12**, 10106. https://doi.org/10.1038/s41598-022-14214-w (2022).
31. Bai, J. *et al.* One-pot synthesis of self S-doped porous carbon for efficient CO_2 adsorption. *Fuel Process. Technol.* **244**, 107700. https://doi.org/10.1016/j.fuproc.2023.107700 (2023).
32. Thammasri, W., Jantrasee, R., Chaiprapa, J. & Jantrasee, S. Electrochemical properties of activated carbon from waste coffee grounds with hydrothermal-microwave radiation technique. *J. Mater. Sci. Mater. Electron.* **34**(7), 595. https://doi.org/10.1007/s10854-023-09963-x (2023).
33. Trinh, K. T. & Tsubota, T. Supercapacitors composed of Japanese cedar bark-based activated carbons with various activators. *Mater. Chem. Phys.* **307**, 128148. https://doi.org/10.1016/j.matchemphys.2023.128148 (2023).
34. Khuong, D. A., Saza, S. & Tsubota, T. The production of high-value products derived from bamboo by steam pretreatment: Sugar-contained water solution and solid residue as a precursor for EDLC electrode. *Mater. Chem. Phys.* **304**, 127853. https://doi.org/10.1016/j.matchemphys.2023.127853 (2023).
35. Kayiwa, R., Kasedde, H., Lubwama, M. & Kirabira, J. B. Mesoporous activated carbon yielded from pre-leached cassava peels. *Bioresour. Bioprocess.* **8**, 53. https://doi.org/10.1186/s40643-021-00407-0 (2021).
36. Nandi, R., Jha, M. K., Guchhait, S. K., Sutradhar, D. & Yadav, S. Impact of KOH activation on rice husk derived porous activated carbon for carbon capture at flue gas alike temperatures with high CO_2/N_2 selectivity. *ACS Omega* **8**, 4802–4812. https://doi.org/10.1021/acsomega.2c06955 (2023).
37. Wang, L. *et al.* Sequential H_3PO_4–CO_2 assisted synthesis of lignin-derived porous carbon: CO_2 activation kinetics investigation and textural properties regulation. *Renew. Energy* **191**, 639–648. https://doi.org/10.1016/j.renene.2022.04.036 (2022).
38. El-Nemr, M. A., Hassaan, M. A. & Ashour, I. Formation of self-nitrogen-doping activated carbon from Fish/sawdust/$ZnCl_2$ by hydrothermal and pyrolysis for toxic chromium adsorption from wastewater. *Sci. Rep.* **13**, 11556. https://doi.org/10.1038/s41598-023-38697-3 (2023).
39. Kwiatkowski, M., Hu, X. & Pastuszyński, P. Analysis of the influence of activated carbons' production conditions on the porous structure formation on the basis of carbon dioxide adsorption isotherms. *Materials* **15**, 7939. https://doi.org/10.3390/ma15227939 (2022).
40. Bedia, J., Peñas-Garzón, M., Gómez-Avilés, A., Rodriguez, J. J. & Belver, C. Review on activated carbons by chemical activation with $FeCl_3$. *C.* **6**(2), 21. https://doi.org/10.3390/c6020021 (2020).
41. Gómez-Avilés, A., Peñas-Garzón, M., Belver, C., Rodriguez, J. J. & Bedia, J. Equilibrium, kinetics and breakthrough curves of acetaminophen adsorption onto activated carbons from microwave-assisted $FeCl_3$-activation of lignin. *Sep. Purif. Technol.* **278**, 119654. https://doi.org/10.1016/j.seppur.2021.119654 (2021).
42. Bedia, J., Belver, C., Ponce, S., Rodriguez, J. & Rodriguez, J. J. Adsorption of antipyrine by activated carbons from $FeCl_3$-activation of Tara gum. *Chem. Eng. J.* **333**, 58–65. https://doi.org/10.1016/j.cej.2017.09.161 (2018).
43. Brunauer, S., Emmett, P. H. & Teller, E. Adsorption of gases in multimolecular layers. *J. Am. Chem. Soc.* **60**, 309–319. https://doi.org/10.1021/ja01269a023 (1938).
44. Galarneau, A., Villemot, F., Rodriguez, J., Fajula, F. & Coasne, B. Validity of the t-plot method to assess microporosity in hierarchical micro/mesoporous materials. *Langmuir* **30**, 13266–13274. https://doi.org/10.1021/la5026679 (2014).
45. He, Y. *et al.* Estimation of shale pore-size-distribution from N_2 adsorption characteristics employing modified BJH algorithm. *Petrol. Sci. Technol.* **39**, 19–20. https://doi.org/10.1080/10916466.2021.1971716 (2021).
46. Ustinov, E. A., Do, D. D. & Fenelonov, V. B. Pore size distribution analysis of activated carbons: Application of density functional theory using nongraphitized carbon black as a reference system. *Carbon* **44**, 653–663. https://doi.org/10.1016/j.carbon.2005.09.023 (2006).
47. Zelenka, T., Horikawa, T. & Do, D. D. Artifacts and misinterpretations in gas physisorption measurements and characterization of porous solids. *Adv. Colloid Interface Sci.* **311**, 102831. https://doi.org/10.1016/j.cis.2022.102831 (2023).
48. Neimark, A. V., Lin, Y., Ravikovitch, P. I. & Thommes, M. Quenched solid density functional theory and pore size analysis of micromesoporous carbons. *Carbon* **47**, 1617–1628. https://doi.org/10.1016/j.carbon.2009.01.050 (2009).
49. Kwiatkowski, M., Fierro, V. & Celzard, A. Numerical studies of the effects of process conditions on the development of the porous structure of adsorbents prepared by chemical activation of lignin with alkali hydroxides. *J. Colloid Interface Sci.* **486**, 277–286. https://doi.org/10.1016/j.jcis.2016.10.003 (2017).
50. Kwiatkowski, M., Gómez-Delgado, E., Nunell, G. V., Bonelli, P. R. & Cukierman, A. L. Mathematical analysis of the effect of process conditions on the porous structure development of activated carbons derived from Pine cones. *Sci. Rep.* **12**, 15301. https://doi.org/10.1038/s41598-022-19383-2 (2022).
51. Kwiatkowski, M., Kalderis, D., Tono, W. & Tsubota, T. Numerical analysis of the micropore structure of activated carbons focusing on optimum CO_2 adsorption. *J. CO2 Util.* **60**, 101996 (2022).

Author contributions

MK: the co-development of the concept of the work, the preparation of the theoretical introduction, the performance of calculations with the use of clustering-based adsorption analysis method (LBET) and the quenched solid density functional theory (QSDFT), the performance of all the figures and table for LBET and QSDFT calculations results, the interpretation and discussing of the results, the writing and co-editing of the manuscript, the corresponding with the editor, the co-replying to reviews and the co-acquisition of the financial support for the project leading to this publication; CB: the co-development of the concept of the work, the performing data collection, the validate data and the co-acquisition of the financial support for the project leading to this

publication; JB: the co-development of the concept of the work, the project administration, the research planning, the co-editing of the manuscript, the co-replying to reviews and the co-acquisition of the financial support for the project leading to this publication.

Funding

This research was funded by a research subvention from the Polish Ministry of Education and Science for the AGH University of Krakow No. 16.16.210.476 and by MCIN/AEI/https://doi.org/10.13039/501100011033 and EU "NextGenerationEU"/PRTR" through project TED2021-129948B-I00.

Competing interests

The authors declare no competing interests.

Additional information

Correspondence and requests for materials should be addressed to M.K.

Reprints and permissions information is available at www.nature.com/reprints.

Publisher's note Springer Nature remains neutral with regard to jurisdictional claims in published maps and institutional affiliations.